

Computation of clear-air radar backscatter from numerical simulations of turbulence:

2. Backscatter moments throughout the lifecycle of a Kelvin-Helmholtz instability

David C. Fritts,¹ Patricia M. Franke,² Kam Wan,¹ Tom Lund,¹ and Joe Werne¹

Received 10 June 2010; revised 27 December 2010; accepted 13 January 2011; published 2 June 2011.

[1] Franke et al. (2011) describe a numerical simulation of the instability and turbulent breakdown of Kelvin-Helmholtz (KH) billows at a high Reynolds number, numerical assessment of radar backscatter, and accuracies of inferred Doppler spectral moments for one test volume. Those results suggest a potential for significant measurement biases for radars that obtain backscatter from refractive index fluctuations. We present in this paper the morphology of computed radar moments throughout the KH instability lifecycle for two radar configurations in order to reveal the evolving character of radar backscatter and compare the radar velocity estimates with true velocities throughout the evolution, and to provide guidance, and cautions, for the interpretation of these dynamics in observational data. Results reveal strong variations in backscatter moments and character, and dependence on radar measurement parameters, that should be beneficial in the interpretation of such measurements in the atmosphere. Backscatter power predictions agree reasonably with observations of such events and their temporal evolutions. Our results also reveal a potential for significant measurement or sensitivity biases, some of which were predicted previously. Examples include a lack of significant backscatter power in well-mixed billow cores, suggesting possibly weak turbulence where in fact it may be strongest, maximum backscatter power in the billow exteriors, where refractive index fluctuations are large but turbulence is weak, underestimated vertical velocities within the KH billows at early times, and inferred significant vertical velocities where true vertical velocities are near zero at late stages of restratification, especially in the edge regions of the turbulence layer.

Citation: Fritts, D. C., P. M. Franke, K. Wan, T. Lund, and J. Werne (2011), Computation of clear-air radar backscatter from numerical simulations of turbulence: 2. Backscatter moments throughout the lifecycle of a Kelvin-Helmholtz instability, *J. Geophys. Res.*, 116, D11105, doi:10.1029/2010JD014618.

1. Introduction

[2] Kelvin-Helmholtz (KH) instability is one of the most common causes of turbulence throughout the atmosphere from Earth's surface to the lower thermosphere. It is of meteorological interest because it contributes vertical mixing of heat, momentum, and constituents, it acts to limit the maximum shears that can occur and the amplitudes of motions contributing these shears, it poses flight risks for aircraft in extreme cases, it impacts optical propagation in laser and astronomical applications, and it creates much of the persistent small-scale turbulence, and associated refractive index variations, that enable us to measure atmospheric flows with various radars. KH instability also plays an

important role in the small-scale dynamics of the oceans. As such, it has received considerable research attention in the past, and it remains an area of active research interest (see *Woods and Wiley* [1972], *Thorpe* [1973a, 1973b], *Fritts and Rastogi* [1985], and *Thorpe* [1987] for reviews of earlier observations and *Fritts and Alexander* [2003] and *Peltier and Caulfield* [2003] for discussions of more recent results).

[3] KH billow wavelengths and depths span a wide range of scales throughout the atmosphere. Maximum wavelengths are as large as several to 10s of km at all altitudes, minimum wavelengths leading to turbulence vary from a few meters or less in the planetary boundary layer, where kinematic viscosity is small, to 10s of meters in the stratosphere and 100s of meters or greater in the mesosphere and lower thermosphere (MLT) [*Witt*, 1962; *Browning*, 1971; *Gossard et al.*, 1971; *Røyrvik*, 1983; *Fritts and Rastogi*, 1985; *Eaton et al.*, 1995; *Chilson et al.*, 1997; *Blumen et al.*, 2001; *Hecht*, 2004; *Hecht et al.*, 2005; *Kelley et al.*, 2005; *Lehmacher et al.*, 2007; *Luce et al.*, 2007, 2008; *Woodman et al.*, 2007]. Billow development depends on

¹Colorado Research Associates Division, NorthWest Research Associates, Boulder, Colorado, USA.

²Department of Electrical and Computer Engineering, University of Illinois at Urbana-Champaign, Urbana, Illinois, USA.

various parameters, most critically the Richardson number, $Ri = N^2/U_z^2$ (where N is the buoyancy frequency and U_z is the vertical shear of the horizontal wind), which measures the tendency for the available kinetic energy in wind shear to overcome the stabilizing influences of stratification, and the Reynolds number, $Re = U_0 h/\nu$ (where U_0 and h are the half velocity difference and the half shear depth, respectively and ν is kinematic viscosity). Values of Ri close to zero favor strong instability, deep billows ($\sim 1/2$ the horizontal wavelength), and relatively intense turbulence, whereas values of Ri closer to $1/4$ favor weak instability, shallow billows, a very different instability and turbulence evolution, and much less intense turbulence [Thorpe, 1973a; Werne et al., 2005]. Values of Re less than a few hundred tend to remain laminar, independent of Ri . However, values of Re of ~ 1000 or greater, especially at lower Ri , favor rapid instability growth and strong three-dimensional (3D) turbulence [Klaassen and Peltier, 1985, 1991; Thorpe, 1987; Fritts et al., 1996, 2003; Smyth, 1999; Werne and Fritts, 1999a, 2001]. One must nevertheless be careful in relying on simple linear theory in assessing KH or other instability dynamics in stratified and sheared flows, as the linear eigenmodes are not orthogonal, allowing for other “optimal” perturbations to occur. Despite the potential for such optimal perturbations, those modes we see most often (or recognize!) at finite amplitude appear to be consistent with guidance from linear asymptotic theory, though signatures of local optimal solutions are apparent in the billow cores at early stages of the KH evolutions described by Werne et al. [2005]. Further discussion of KH instability dynamics is provided in the reviews by Thorpe [1987] and Fritts and Alexander [2003] and references therein [see also Peltier and Caulfield, 2003].

[4] KH instability is a major cause of the turbulence that enables radar backscatter at frequencies ranging from MF to UHF. MF and HF systems (typically ~ 2 to 3 MHz), either spaced antenna or Doppler, are sensitive to altitudes from ~ 60 to 100 km, while VHF (~ 50 and 224 MHz) and UHF (~ 430 MHz and ~ 1 GHz) systems are employed for measurements from Earth’s surface into the thermosphere. At higher frequencies and/or higher altitudes, however, free electrons, and elevated electron density fluctuations (due to high Schmidt numbers under summer mesopause conditions), and/or sharp electron density gradients are necessary to enhance refractive index fluctuations due to neutral densities and achieve useful measurements [Balsley and Gage, 1980; Röttger, 1994; Cho and Röttger, 1997; Lübken et al., 1998; Hill and Mitton, 1998; Hill et al., 1999]. We note that some of the radars that rely on refractive index fluctuations at lower altitudes (typically the VHF and UHF frequencies, ~ 50 , 224 , and 430 MHz and above) also obtain incoherent scatter returns at MLT altitudes that are not likely to be sensitive to the biases that are the subject of this paper. They are, nevertheless, capable of measuring the same dynamics and may, therefore, be in a position to contribute to a more complete understanding of these measurement biases.

[5] Whether backscatter occurs primarily due to neutral density fluctuations in the lower atmosphere or to electron density fluctuations at higher altitudes, correlations of the refractive index fluctuations with the underlying dynamics have been implicated in a number of measurement biases noted to date. Several authors have noted a potential for

biases in radar Doppler wind measurements [Kudeki et al., 1993; Muschinski, 1996, 2004; Muschinski et al., 1999; Gibson-Wilde et al., 2000; Tatarskii and Muschinski, 2001; Worthington et al., 2001]. Others have reported mean vertical motions that differ from expectations in both sign and magnitude [Balsley and Riddle, 1984; Nastrom et al., 1985; Fritts and Yuan, 1989; Meek and Manson, 1989; Rüster and Reid, 1990; Wang and Fritts, 1990; Fritts et al., 1990; Fukao et al., 1991]. Specifically, Nastrom and VanZandt [1994] suggested that a bias toward negative mean vertical velocities resulted from a correlation between higher radar backscatter power with the higher refractive index fluctuations accompanying the downward (more stable and with reduced high-frequency velocity variance) phases of the gravity waves (GWs) modulating atmospheric stability and turbulence intensities. Hoppe et al. [1990] and Hoppe and Fritts [1995a, 1995b] assessed the correlations between backscatter power, vertical velocity, and spectral width using the EISCAT 224 MHz radar under polar mesosphere summer echo (PMSE) conditions and found high power to be well correlated, in general, with narrow spectral widths and downward motions. Hoppe et al. [1990] also noted similar correlations using the SOUSY 53.5 MHz radar. These latter studies, employing neutral and electron fluctuations, suggest that the downward phase of GW motions, where we expect turbulence to be weak or decaying [Fritts et al., 2009a, 2009b], enables sharper gradients, higher backscatter power, suppressed vertical motions, and narrower spectral widths than in the upward, and less stable, phase of the GW motion. Tatarskii and Muschinski [2001] provided a theoretical framework demonstrating that differences between real and measured radial velocities arise due to correlations between radial velocity and refractive index fluctuations, with potential additional contributions due to higher-order correlations.

[6] Measurement biases accompanying radar observations of KH instability were first suggested by Muschinski [1996], who argued that the systematic slopes of layered features accompanying KH evolution in mean shear could lead to errant vertical velocity estimates. Other biases are suggested by many observations of the familiar Kelvin’s “cat’s eye” structures in radar backscatter power, which clearly delineate the KH billows but appear to fail to capture the stronger turbulence often occurring within the billow cores [see Fritts and Rastogi, 1985, and references therein; Fritts et al., 2003]. The more recent spectacular measurements of such structures in the boundary layer, the troposphere, and the MLT by Eaton et al. [1995], Woodman et al. [2007], Lehman et al. [2007], and Luce et al. [2008] provide additional compelling evidence of the prevalence and character of such dynamics throughout the atmosphere.

[7] The first detailed assessment of such biases by Gibson-Wilde et al. [2000] employed a direct numerical simulation (DNS) of KH instability at an initial $Re = 2000$, and the isotropic plasma turbulence model developed by Hill and Mitton [1998] and Hill et al. [1999] extending refractive index fluctuations to smaller spatial scales, to evaluate the classical theories and assumptions related to mixing and energy dissipation rates in stratified flows [Weinstock, 1981]. The result was that the theory, and its predictions, appear to have major deficiencies because the underlying assumptions (i.e., that turbulence is stationary,

homogeneous, and isotropic) are not an accurate description of the turbulent flow due to KH instability in a sheared and stratified fluid at any stage in its evolution.

[8] The potential for biases in radar measurements arises from the departures of turbulence from isotropy and homogeneity during both its active and decaying phases in stratification and shear, and its influences on laminae that may contribute nonturbulent radar backscatter. Departures from turbulence isotropy due to stratification and shear were first addressed theoretically by *Uberoi* [1957], *Townsend* [1959], *Bolgiano* [1959, 1962], and *Lumley* [1964]. Reviews of early work addressing turbulence anisotropy were provided by *Champagne* [1978], *Mestayer* [1982], *Browne et al.* [1987], *Hunt et al.* [1991], *Sreenivasan* [1991], and *Van Atta* [1991]. More recent experimental, numerical, and theoretical studies further quantified our understanding of the departures from isotropy due to shear and/or stratification for various geophysical flows [*Durbin and Speziale*, 1991; *Werne and Fritts*, 1999a, 1999b, 2000, 2001; *Smyth and Moum*, 2000; *Pettersson-Reif et al.*, 2002; *Fritts et al.*, 2003; *Pettersson-Reif and Andreassen*, 2003; *Wroblewski et al.*, 2003; *Ruggiero et al.*, 2005; *Werne et al.*, 2005, *Fritts et al.*, 2009a, 2009b].

[9] The companion paper by *Franke et al.* [2011] (hereafter F11) employs the Born approximation computed in the time domain for radar backscatter developed for isotropic turbulence by *Tatarskii* [1961, 1971] and extended to more general anisotropic turbulence and Fresnel backscatter by *Doviak and Zrnik* [1984], *Muschinski et al.* [1999], and *Muschinski* [2004]. Backscatter power and mean Doppler shift are computed for representative turbulence volumes defined by a large-eddy simulation (LES) of KH instability at $Re = 10,000$ (evaluated for realistic descriptions of turbulence against our DNS simulations at $Re = 2500$) and compared with vertical velocities obtained directly from the LES data described by F11. These comparisons reveal a potential for radar measurement biases that depend on measurement parameters and the character of the turbulence field.

[10] Our purposes in this paper are to employ the LES description of turbulence due to KH instability and the method for computation of radar backscatter described by F11 to exhibit expected radar responses throughout the life cycle of a KH instability. Specifically, we assess radar backscatter power and the first moment of the Doppler spectrum for an assumed vertical beam and compare the vertical velocities computed directly (without radar biases) from the same LES volumes. These comparisons indicate (1) that radar backscatter power is dominated by regions within the evolving KH billow and turbulence layer having large refractive index gradients (and C_n^2), with relative insensitivity to the regions of strongest turbulence within the well mixed billow cores and (2) that biases in radar estimates of vertical velocities occur throughout the active and decaying phases of KH instability and may impact interpretations of both instability dynamics and mean motions. Our assumptions for the character of the KH instability evolution, the environment in which it occurs, and the radar sampling parameters are described in section 2. We show in sections 3 and 4 how this evolution would appear as viewed by 10 and 3 MHz radars having very high spatial resolution and vertical beams. In these applications, the 10 MHz

sampling frequency is employed as a surrogate for higher-frequency VHF systems at MLT altitudes in order to describe sampling volumes and KH spatial scales within the resolution constraints of our modeling capabilities. These same results allow computation of equivalent 50 MHz responses to the same KH dynamics in the lower stratosphere (assuming high radar bandwidth and spatial resolution) because of the much smaller typical scales of these dynamics (and the higher effective simulated spatial resolution) at these altitudes. Section 4 provides our summary and conclusions.

2. Backscatter Environment and Virtual Radar Measurement Parameters

[11] Following F11, we assume radar backscatter from the life cycle of a KH instability described by an LES description of KH instability evolution for $Ri = 0.05$, $Re = 10^4$, and a Prandtl number $Pr = \nu/\kappa = 1$. We assume KH and radar parameters appropriate to higher levels of the atmosphere, where effects of humidity can be neglected. KH instability occurs for plane parallel shear flows for which $Ri < 1/4$, so our chosen Ri allows for rapid and vigorous instability development. A large Re also allows for rapid breakdown of the KH billows (or cat's eyes) via secondary instabilities arising initially in the billow exteriors that lead to turbulence generation, penetration throughout the billow, shearing of the billows to a horizontally uniform turbulence layer, and eventual restratification as turbulence subsides. Additional details are provided by F11 and references therein. For our simulation, the initial horizontal mean wind is given by $U(z) = U_o \tanh(z/h)$, with $U_o = 5 \text{ m s}^{-1}$ and $h = 150 \text{ m}$, such that $U_z = U/h = 0.0333 \text{ s}^{-1}$, the KH instability has a most unstable horizontal wavelength $L = 12.566 h$, and the billow and turbulence layer will approach a typical depth of $D \sim 6h \sim 900 \text{ m}$ and allow radar sampling representative of such measurements in the MLT. The quantities ν and κ are kinematic viscosity and thermal diffusivity, respectively, and have true atmospheric values for KH billow wavelengths of $\sim 75 \text{ m}$, 750 m , and 7.5 km at altitudes of ~ 30 , 60 , and 90 km , respectively. Pr differs from that of the atmosphere, ~ 0.7 , however, in order to achieve uniform resolution requirements in the velocity and potential temperature fields. These choices imply a time scale h/U , a buoyancy frequency $N = Ri^{1/2}/30 \sim 0.0075 \text{ s}^{-1}$, and a buoyancy period $T_b = 2\pi/N = 28h/U = 843 \text{ s}$ ($\sim 14 \text{ min}$). The LES was performed in a computational domain with streamwise, spanwise, and vertical dimensions of $(12.566, 4.2, 25)L$, and employed spatial resolution of $(720, 240, 1440)$ spectral modes, yielding vertical resolution of $\Delta z \sim 2.6 \text{ m}$ to ensure sufficient resolution of structures at the assumed radar Bragg scales of 15 and 50 m for our radar backscatter assessments. To ensure resolved radar phase variations and Doppler velocities, we chose a sampling interval of 1.5 s and 64 samples per spectral computation. This implies a sampling interval of 96 s or $\sim 0.11 T_b$.

[12] Radar backscatter assessments were performed for two radar frequencies for which the LES described by F11 provides explicit resolution of the Bragg scales. Our first assessment of radar backscatter characteristics and accuracy is performed with the following assumptions: (1) a 10 MHz Doppler radar with a narrow vertical transmit beam having a

Table 1. Radar Frequency and Resolution Combinations Assessed in This Paper

Radar Frequency	Bragg Scale	Pulse Width	Vertical Resolution	Beam Width
(Case A) 10 MHz	15 m, 6 Δz	90 m, 36 Δz	45 m, 18 Δz	180 m
(Case B) 10 MHz	15 m, 6 Δz	300 m, 120 Δz	150 m, 60 Δz	180 m
(Case C) 3 MHz	50 m, 20 Δz	300 m, 120 Δz	150 m, 60 Δz	300 m

($\sin x$)/ x shape, a main lobe full width of 180 m with sidelobes suppressed, and a broad receive beam; (2) a radar baud length yielding a Gaussian full-width, half-maximum (FWHM) pulse width of 90 m (and an altitude resolution of 45 m); (3) the radar samples successive spatial positions within the KH billow, separated by the full beam width in the streamwise direction, simultaneously in order to achieve the optimal definition of the KH billow structure and evolution in space and time; (4) measurements are assumed invalid due to low S/N if backscatter power is less than 1% of the maximum within each field; and (5) the moments of the Doppler spectrum can be assessed using the method described by F11.

[13] This set of radar parameters will be referred to as Case A. A second set differing from Case A only in the pulse length (increased from 6 to 20 Bragg scales) will be referred to as Case B. Finally, Case C comprises parameters representing a 3 MHz radar frequency, a 50 m Bragg scale, a 300 m (FWHM) pulse width, and a 300 m full width of the primary beam. The radar parameters for each of these cases are listed in Table 1 for ease of comparison.

[14] We choose times of $t = 37, 54, 84, 129, 256, 312,$ and $364 h/U_o$, spanning $\sim 12 T_b$, to illustrate the KH evolution from the late 2D flow through the turbulence transition, billow mixing and breakdown, and formation and restratification of the turbulence layer at late times. Streamwise-vertical cross sections of potential temperature, vertical velocity, and vorticity magnitude, for these times are shown in Figure 1 for reference.

3. Simulated 10 MHz Backscatter Moments

3.1. High-Resolution Measurements in Altitude at 10 MHz (Case A)

[15] Backscatter power obtained for each of the times displayed in Figure 1 is shown in Figure 2a for the assumed radar beam configuration described above (denoted A in Table 1). Corresponding vertical velocities are shown in Figure 2b. For all fields, range cells for which the backscatter power is less than 1% of the maximum power within the field are assumed unable to yield valid Doppler velocity estimates and are shown as gray cells indicating no data. Considering first the backscatter power, we see that the dominant returns come, in all cases, from the billow or turbulence layer edge regions. At the earliest times ($t = 37$ and 54), backscatter is relatively strong but occurs only where potential temperature gradients are large, relatively coherent, and aligned nearly vertically, as there are developing instability structures at $t = 54$, and strong gradients projecting onto the 15 m Bragg scale, but no turbulence inertial range at these times. At intermediate times ($t = 84$ and 129), turbulence is well developed within the outer billow or the billow core itself, backscatter power is now much weaker, and it maximizes at the outer edges of the billow and turbulence layer and decreases strongly within

the billow core. It is only at the latest times ($t = 256$ and after) that backscatter power suggests that the turbulence is finally achieving a quasi-horizontally homogeneous state, and in the later stages of restratification ($t = 312$ and 364) that backscatter power becomes significant within the turbulence layer. Significant backscatter power also persists in the edge regions where discernable gradients at the Bragg scale are seen to persist in the potential temperature field due to continued shearing of tilted layers.

[16] Given these results, what are the implications for scattering processes for these radar parameters? At the earliest time, the dominant backscatter power occurs where Bragg-scale quasi-coherent flow structures are nearly horizontal and must contribute largely through specular backscatter. The backscatter at this time is quite strong, suggesting that specular contributions to total power may dominate when they occur. At intermediate times ($t = 84$ and 129), turbulence is well developed and has largely eradicated thermal and refractive index gradients within the billow. This results in the dominant backscatter accompanying the smaller turbulence intensities within the re-formed thermal gradients within the billow edge regions. Backscatter power is also highest where these gradients are more nearly horizontally aligned than where the quasi-2D dynamics impose significant slopes. At these times, there is strong turbulence, first in the outer billow and later throughout the entire billow and at all horizontal locations, though it requires $\sim 1 T_b$ for turbulence to penetrate into the billow core and another $\sim 2 T_b$ for the turbulence layer to become nearly horizontally homogeneous (see Figure 1). At later times, both the surviving turbulence and the large-scale potential temperature gradients become more uniform horizontally, and radar backscatter is more uniform horizontally, suggesting that specular reflections are again making significant contributions to total backscatter.

[17] Vertical velocities obtained from the first moments of the Doppler spectrum for each LES data set for Case A parameters are shown in Figure 2b. The true vertical velocity field sampled with the same spatial weighting, and the differences between the true and radar velocities, are shown at the same times for comparison in Figures 2c and 2d. The top panel indicates nonzero velocity estimates only where there is sufficient backscatter power in the billow edge regions, and these estimates, while small, are relatively good approximations to the true velocities at this time. The next three panels ($t = 54, 84,$ and 129) exhibit relatively coherent upward and downward motions at the left and right sides at times during which the billow is fairly coherent, and spanning turbulence formation and mixing of the billow core. The velocity estimates fail to capture the true velocity maxima within the billow core at these times, however, suggesting a lack of sensitivity to motions where refractive index variations are weak or have been largely destroyed by mixing, despite backscatter power above our 1% threshold

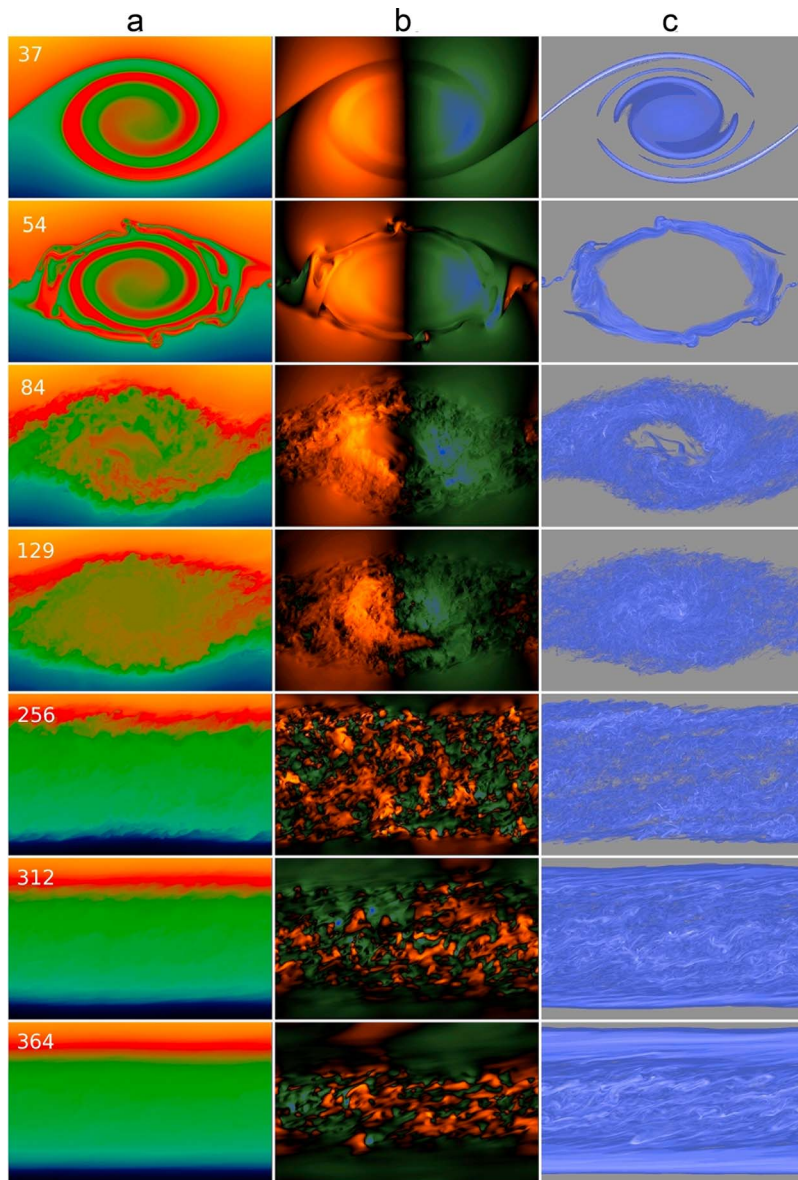


Figure 1. (a) Streamwise-vertical cross sections of potential temperature, (b) vertical velocity, and (c) vorticity magnitude, for the KH LES described by F11 at $t = 37, 54, 84, 129, 256, 312,$ and 364 (shown at top left in Figure 1a panels for convenience) spanning $\sim 12 T_b$.

at $t = 84$ and beyond. Indeed, the radar velocities systematically underestimate the true velocities at all locations (the velocity differences and true velocities are highly correlated from $t = 37$ to 129) except in a thin region corresponding closely to the region of highest backscatter power at each

time from $t = 54$ to 129. In the core region the radar tends to underestimate the velocities for several reasons: a lack of backscatter at the Bragg scale where velocities are large, the averaging effect of the pulse, and difficulty in measuring velocity when the velocity (and power) vary significantly

Figure 2. (a) Backscatter power and (b) Doppler velocities obtained for a radar frequency of 10 MHz, a Bragg scale of $6 \Delta z$ (~ 15 m), and a pulse length of $36 \Delta z$ (a vertical resolution of ~ 45 m) using the methodology of, and for the KH evolution described by, F11 at the times displayed in Figure 1 (shown in Figure 1a for convenience). Doppler spectra employed 64 samples at 1.5 s intervals at each time. The beam width (FWHM) was assumed to be 180 m in the streamwise direction with a $\sin(x)/x$ weighting, and the full spanwise width of the KH simulation. (c) The true vertical velocities weighted as in the radar estimates and (d) the true-minus-radar differences. Power and velocity color scales are shown at the bottom of each panel. Range cells with power less than 1% of the maximum in each panel are judged not able to yield valid velocity estimates and are shown as gray.

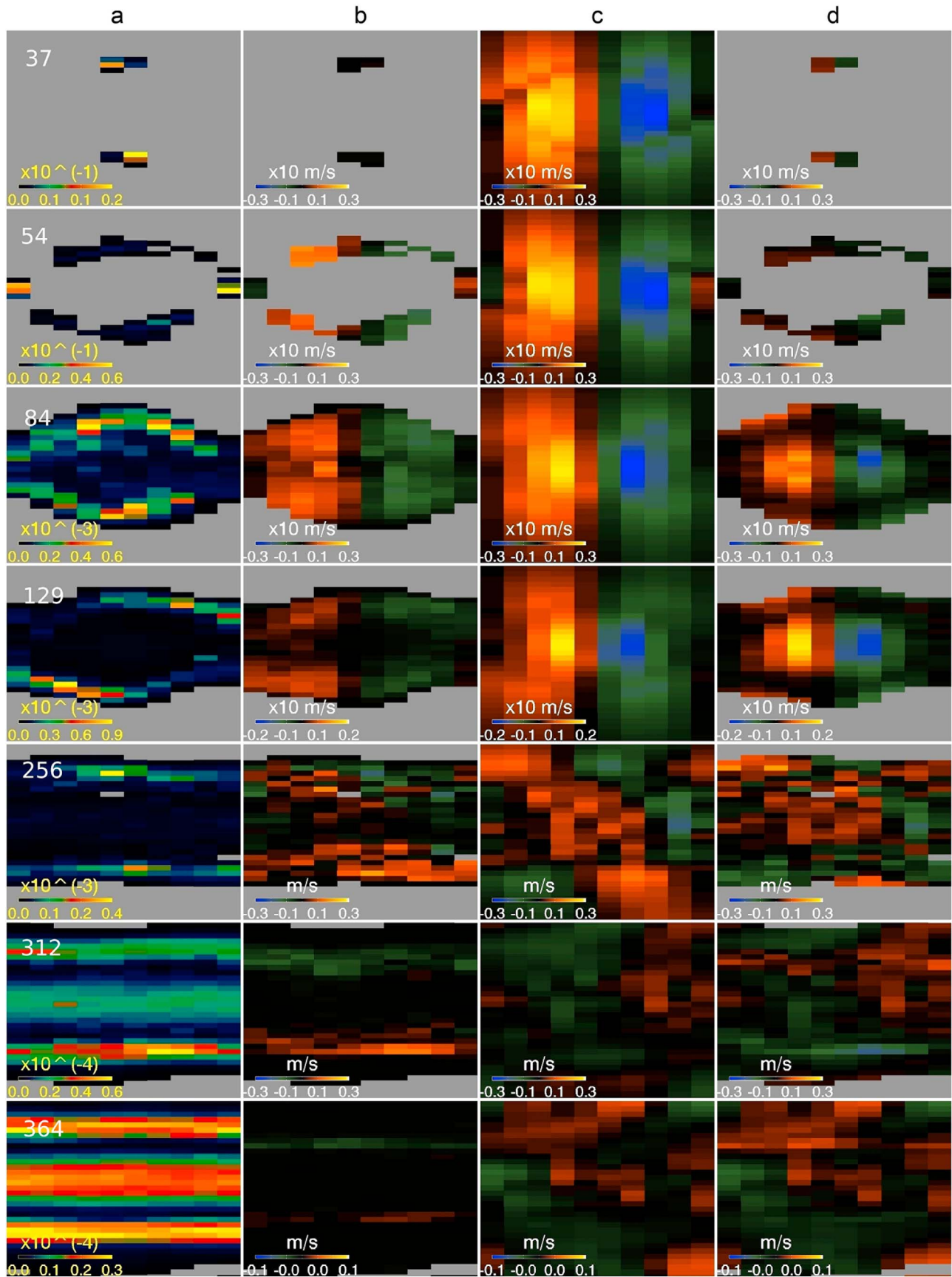


Figure 2

during the time spanned by the spectral assessment. Thus, unbiased velocity estimates at early and intermediate times occur only where backscatter is relatively strong, the velocity is relatively constant, and the Doppler spectrum is well defined.

[18] At later times ($t = 256$ and after), there are both (1) spurious large velocities that are limited in altitude at the upper and lower edges of the decaying turbulence layer and (2) a lack of sensitivity to coherent, larger-scale true motions both within and external to the turbulence layer. Differences outside the billow or turbulence layer at all times occur where there is essentially no small-scale structure and where we should expect little, if any, radar backscatter. These regions nevertheless largely reflect the velocities at the edges of the turbulence layer due to the long tails of the assumed Gaussian radar pulse, when there is sufficient backscatter power. Lack of sensitivity to motions within the turbulence layer at $t = 256$ is a result of the strong mixing and eradication of thermal and refractive index gradients by turbulence that has not yet restratified (see the strong turbulence that persists throughout the layer at this time in the vorticity field in Figure 1c), and because the velocity of the fluid varies greatly in the turbulent layer. The significant radar vertical velocities at the edges of the turbulence layer at late times ($t = 312$ and 364 , negative at the top and positive at the bottom) arise due to largely horizontal advection of slanted structures yielding specular reflections (seen more clearly in the vorticity than in the potential temperature fields in Figure 1 at these times) that maintain Bragg-scale structure to late times because of continuing shearing of the flow, rather than vertical motions of specific scatterers. Motions in the edge regions are now essentially horizontal ($\sim 5 \text{ m s}^{-1}$, with 3D turbulence structures largely absent) and the relative motion is to the right at the top of the layer and to the left at the bottom. These horizontal motions result in apparent downward (upward) motions at the top (bottom) of the layer due to the slight tilt of the potential temperature structures at these late times (and also seen in the vorticity) that are upward and to the right due to the mean shearing motion of the expanded shear layer.

[19] We now examine the character of the Doppler spectra from which the vertical velocity estimates are obtained. These are compared with the distributions of true vertical velocities within the same scattering volumes, weighted by the radar beam width and pulse length, for two representative locations at early, intermediate, and late times in Figure 3. Figure 3 (top) shows true (solid line) and radar (dashed line) velocity spectra just left of the center of the billow (Figure 3, top left) and in the edge region at the top of the billow just left of center (Figure 3, top right) at $t = 54$, when instability structures are seen in the outer portion of the billow, but turbulence has not yet developed and the billow core is laminar. Figure 3 (top left) exhibits a reasonable correlation, but a biased estimate of the spectral shape, whereas Figure 3 (top right) exhibits almost no correlation between true and radar velocities at this time. True velocities left of the billow center (Figure 3, top right) are large and positive, as noted above, but the radar velocity spectrum exhibits power nearer zero Doppler shift that comes from the strong refractive index variations in the billow edge regions above the sampling altitude due to the Gaussian pulse shape. The spectra

within the upper and lower portions of the billow exhibit significant biases in general (see Figure 2a for these times) because the radar power comes preferentially from the billow edge regions having strong refractive index gradients, and these are not uniformly distributed throughout the sampling volume at these times.

[20] At $t = 129$ (Figure 3, middle), there is considerably better agreement between true and radar velocities, because turbulence is now well developed and fills the sampling volumes. Both in the center of the turbulence layer and toward its upper edge (Figure 3, middle left and middle right), true velocities exhibit spectral widths of $\sim 1 \text{ m s}^{-1}$ and means of ~ 1.8 and 0.8 m s^{-1} . Radar velocity spectra now overlap the true velocities to a significant degree, but the mean radar velocities are ~ 1.5 and 0.6 m s^{-1} , or $\sim 20\%$ less than the true velocities because the Doppler spectral power is again biased toward the edges of the turbulence layer where vertical velocities are smaller. This shows how the radar processing, which depends on the shapes of the Doppler spectra, systematically underestimates velocities, as noted above.

[21] As turbulence decays and the layer restratifies, backscatter power occurs throughout the layer. We expect the model of uniform volume filling turbulence to be valid during this phase, implying that the velocity estimates should be the best at these times. However, we find that systematic biases in radar velocity estimates still occur. The structure of the turbulence suggests that the biases are predominantly the result of the tilting and stretching of thermal and refractive index gradients by the mean shearing motions that accompany restratification. This tendency can be seen clearly in the potential temperature and vorticity fields at $t = 312$ and 364 in Figure 1. The effects are illustrated in Figure 3 (bottom), which are near the lower and upper edges of the turbulence layer. The mean (horizontal) velocities ($\sim 5 \text{ m s}^{-1}$) at these times advect these structures to the left at lower altitudes and to the right at higher altitudes. The effect of this advection (with the slanted character of these gradients having structure at the Bragg scale, see Figure 1c for these times) is an apparent upward (downward) velocity in the lower (upper) edge of the turbulence layer as it restratifies. While the radar Doppler spectrum at the lower edge of the turbulence layer (Figure 1c, last panel) suggests both positive and negative velocities (both of which are outside the range of true velocities at this location), the power at positive velocities dominates, and the mean Doppler velocity is consistent with the apparent upward motion induced by the slanted gradients. The opposite is the case at the upper edge of the turbulence layer, where the dominant power is at negative Doppler velocities and the mean again differs significantly from the true mean velocity. Thus, radar backscatter at late stages in the restratification of a turbulence layer arising from KH shear instability exhibits biases in radar Doppler vertical velocities that are anticipated to yield clear measurement errors that may impact the interpretation of the small-scale dynamics and associated mean motions.

[22] In real applications, we expect finite radar S/N to mask velocity estimates where backscatter is very weak. But this will not preclude the biases noted above due to insensitivity to significant vertical motions within the billow cores, either prior to significant small-scale structures or after mixing and eradication of the refractive index variations. Nor will it avoid biases accompanying horizontal advection of

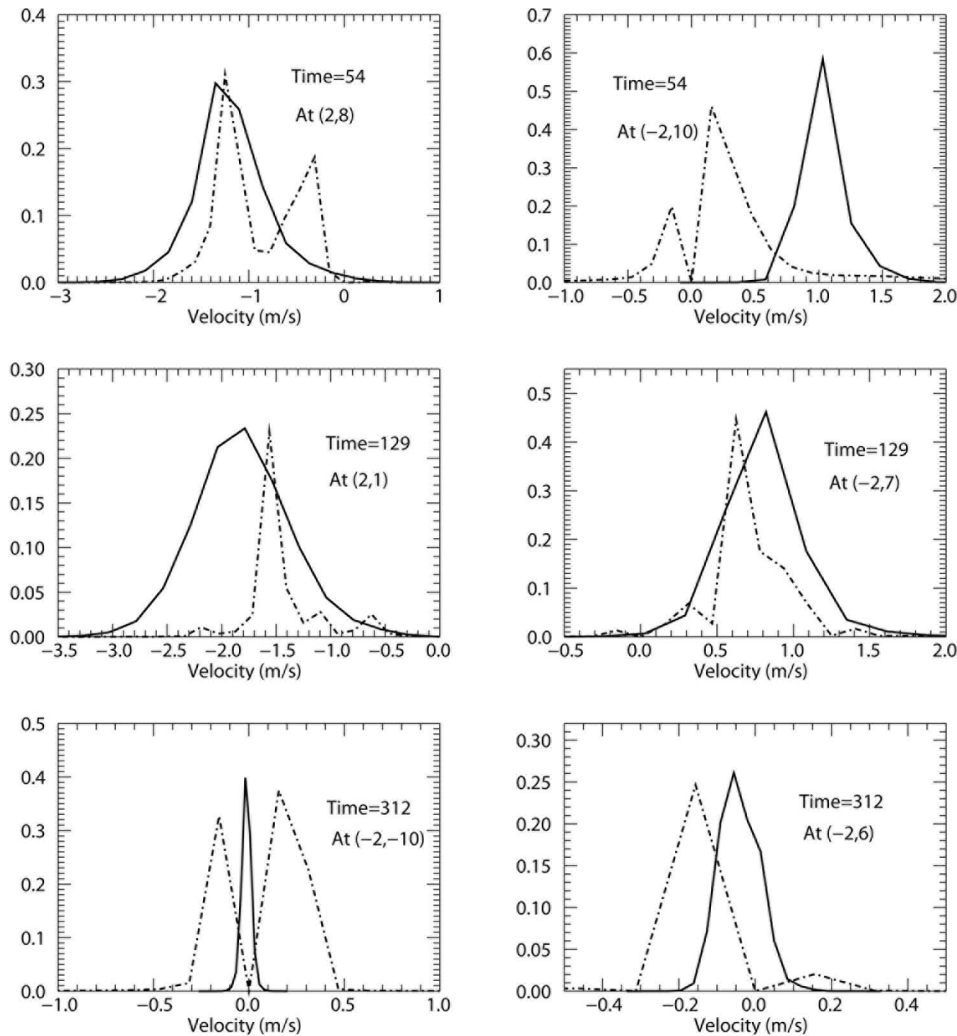


Figure 3. Representative comparisons of Doppler spectra computed by radar backscatter (dash-dotted lines) with the true Doppler velocity distributions within the same sampling volume (solid lines) for the 10 MHz frequency and short pulse length in Case A. Comparisons for (top) $t = 54$, (middle) $t = 129$, and (bottom) $t = 312$. Sample volume locations (x,z) are indicated relative to the center of the initial KH billow relative to a $(0,0)$ position at the center of each image. Note that the major biases accompany specular backscatter where turbulence is weak, but refractive index variations are strong.

slanted specular reflectors at late stages of the evolution. Indeed, these comparisons reveal that radar estimates provide only qualitative information on the large-scale KH velocity field at this spatial resolution and that there is a significant potential for measurement biases (ranging from underestimates of true velocities to apparent radial velocities when true velocities are very small) that could contribute to a misinterpretation of real radar measurements and to inaccurate assessments of the corresponding neutral dynamics, unless more robust radar processing techniques are developed.

3.2. Lower-Resolution Measurements in Altitude at 10 MHz (Case B)

[23] We now examine the results of employing the same radar parameters as in Case A above, but with a sampling pulse that is 300 m (Case B) rather than 90 m FWHM. The

computed radar backscatter power and vertical velocities for Case B corresponding to those obtained in Case A are shown in Figures 4a and 4b, again with power and Doppler velocities not shown for backscatter power less than 1% of the maximum in each frame. These fields exhibit similarities to, and differences from, those shown for Case A, again with the only difference in the two cases being the pulse length. First comparing the backscatter power, we see that the overall fields are very similar, with slightly elevated power in Case B at early and intermediate times, and spatial distributions having common shapes and intensity distributions through $t = 256$, apart from the obvious differences due to spatial resolution. As in Case A, the power distributions for Case B define the billow and turbulence layer outlines reasonably well, though the curved edges of the KH cat's eye structure are less distinct at the coarser resolution. In

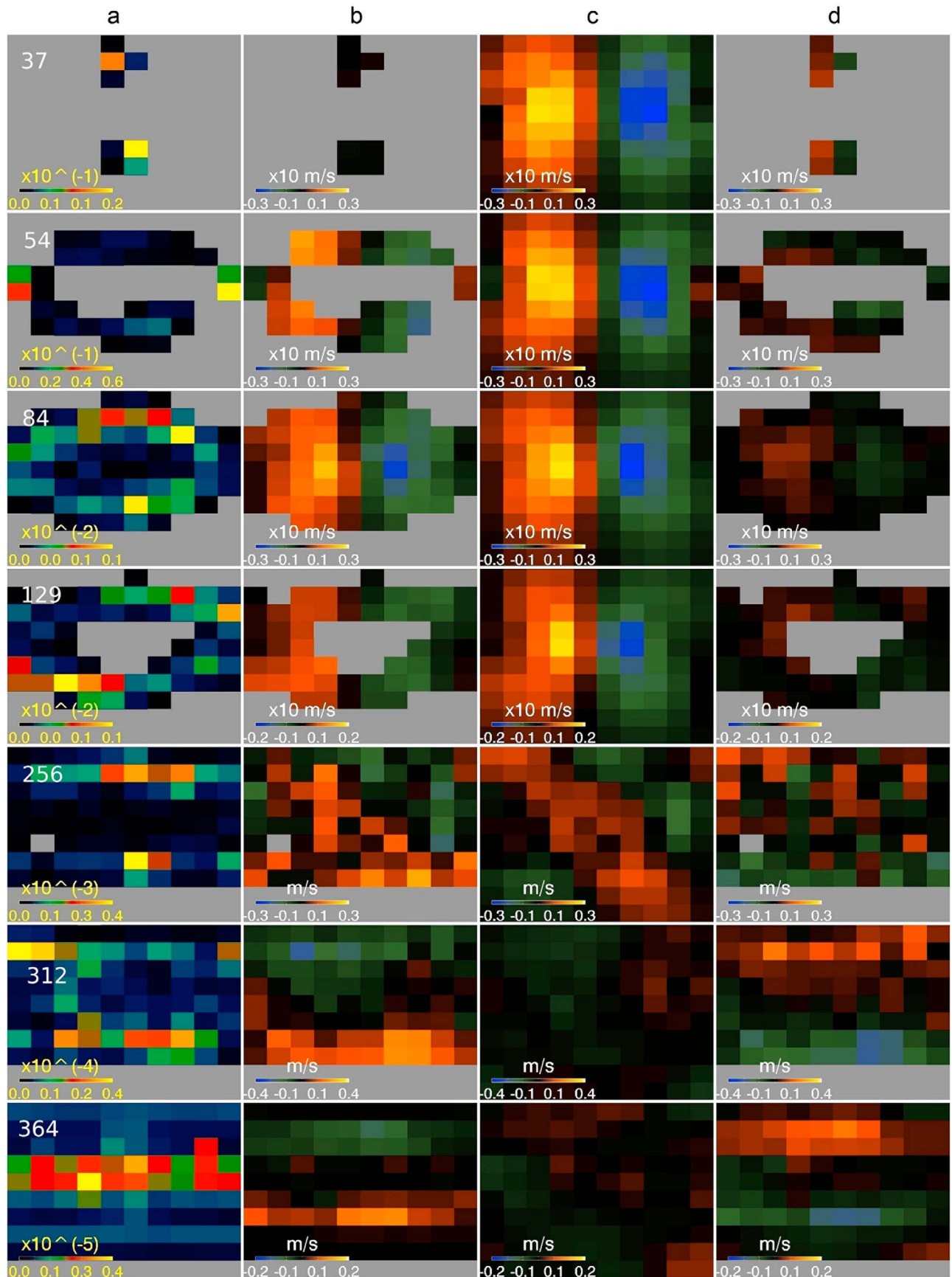


Figure 4. Same as Figure 2 but for a pulse length of $120 \Delta z$ (vertical resolution of ~ 150 m).

neither case does the radar observe significant power in the interior of the billow or the turbulence layer until very late times, and the higher backscatter power in Case B at some locations cause some measurement dropouts within the billow compared to Case A.

[24] As the turbulence layer restratifies ($t = 312$ and 364), the broader pulse results in much less coherent structures in space and time, with isolated regions of high and low power interspersed, where Case A results are more smoothly varying in altitude and the horizontal (compare the sixth and seventh rows in Figure 4 with those in Figure 2). Both cases also exhibit significant relative backscatter power within the turbulence layer as it restratifies, but power levels remain low, and this is likely due to both an increase in stratification in the layer interior and greater coherence among the residual turbulence structures at later stages (see the vorticity images at $t = 312$ and 364 in Figure 1c). Overall, Case A power profiles appear to describe the early and late stages of KH instability evolution and structure more accurately, including the evolution of billow shape, the transition to a more nearly homogeneous turbulence layer, and the late-time restratification. At later stages, the two pulse lengths respond to very different features of the turbulence layer, with Case A capturing both edge and interior regions and Case B less sensitive overall and especially to the turbulence edge regions as the layer restratifies. The latter suggests that coherent Bragg-scale structures at the edges of the turbulence layer at late times have small vertical extent.

[25] Vertical velocities for Case A and Case B are likewise very similar in their gross features, and more similar to each other than either is to the true velocity field at early and late times. There are also some interesting differences, however. At early times ($t = 37$ and 54), neither case achieves sufficient backscatter power to assess vertical velocities in the billow core. At intermediate times ($t = 84$ and 129), the longer radar pulse in Case B does a somewhat better job of defining the velocity field within the KH billow or turbulence layer, presumably because it samples a larger part of the flow so that each scattering volume contains more scatterers. At later times, however, Case B appears to yield velocity estimates exhibiting comparable or greater errors compared to Case A, both in the turbulence edge regions and in the outer flow. Radar Doppler velocities in Case B also fail to capture the larger-scale coherent structures within and external to the turbulence layer, and they imply significant vertical motions in the edge regions (much larger than in Case A) not seen in the true velocity fields at these times due to largely horizontal advection of slanted features in the potential temperature field.

[26] As in Case A, we display several comparisons of Doppler spectra obtained in Case B with the true velocity distributions for early, intermediate, and late times of $t = 54$, 129 , and 312 in Figure 5. The spectra shown in Figure 5 (top) ($t = 54$) are in the second and third rows below the midpoint and just to the right and left of the midpoint, respectively. Each Doppler spectrum appears to be better defined by the larger sampling volume, compared to those examined in Case A. Indeed, the true and radar spectra now span largely the same velocities. The major difference in each Case B spectrum is the power near zero velocity that skews the radar velocity estimate toward zero relative to the true velocity distribution. Doppler spectra at $t = 129$ exhibit

similar biases relative to the true velocities, again with relatively more power at small Doppler velocities because of the higher backscatter at the turbulence layer edge regions. Comparing Doppler and true velocities in the lower and upper portions of the turbulence layer at $t = 312$ (Figure 5, bottom), we see that the biases identified in Case A are again present. Apparent motions due to horizontal advection of the slanted structures and gradients are much larger than the true vertical motions, or the widths of these distributions, at these positions in Case A. Indeed, specular backscatter from slanted reflectors appears to yield systematic vertical velocity biases at late stages of turbulence restratification in mean shear, whether radar spatial resolution is relatively fine or more coarse.

[27] To evaluate the biases accompanying specular backscatter in the turbulence layer at later stages in the KH evolution more completely, we display in Figure 6 (top) the mean vertical velocity profiles obtained by averaging over all horizontal beam positions for Case B at $t = 312$ and 364 . Each profile exhibits maximum positive and negative mean Doppler vertical velocities at the lower and upper edges of the turbulence layer that span two or three altitudes and which are seen to decrease in magnitude with time. These profiles are entirely consistent with the discussion of individual Doppler spectra in Cases A and B above, and the decrease in the biases with time can be traced to the decreasing tilt of the residual layered structures at the Bragg scale seen in the turbulence edge regions with time due to the continued shearing motions. Importantly, however, these biases are ~ 0.05 to 0.15 m s^{-1} at these times, and are thus comparable to, or much larger than, expected mean vertical velocities throughout the atmosphere. These suggest that such biases may contribute significant uncertainties in the use of conventional radar processing techniques to estimate mean vertical motions or mean responses to dynamical processes that may otherwise be adequately described by such measurements.

4. The 3 MHz Measurement Biases and Parameter Dependence

[28] We now examine the backscatter power and vertical velocity fields obtained for a 3 MHz radar having similar characteristics to those described for the 10 MHz radar above, except in this case having a Bragg scale of $20 \Delta z$ (50 m), a pulse length of $120 \Delta z$ (a vertical resolution of 150 m), and a beam width (FWHM) of 300 m . These correspond to Case C in Table 1. The computed radar backscatter power and vertical velocities for Case C corresponding to those obtained in Cases A and B are shown in Figures 7a and 7b.

[29] The backscatter power fields exhibit similarities to, and differences from, those shown for Cases A and B, apart from the obvious differences in spatial sampling. These fields are most similar to those of Case B, but with slightly elevated power at earlier times and significant power enhancements at later times. Backscatter power at $t = 37$ is large and confined to those portions of the flow where the refractive index gradients are large and nearly vertical. Indeed, the 3 MHz Bragg scale is obviously much better matched to the billow thermal structures than the 10 MHz Bragg scale at this time. Case C power differs from the

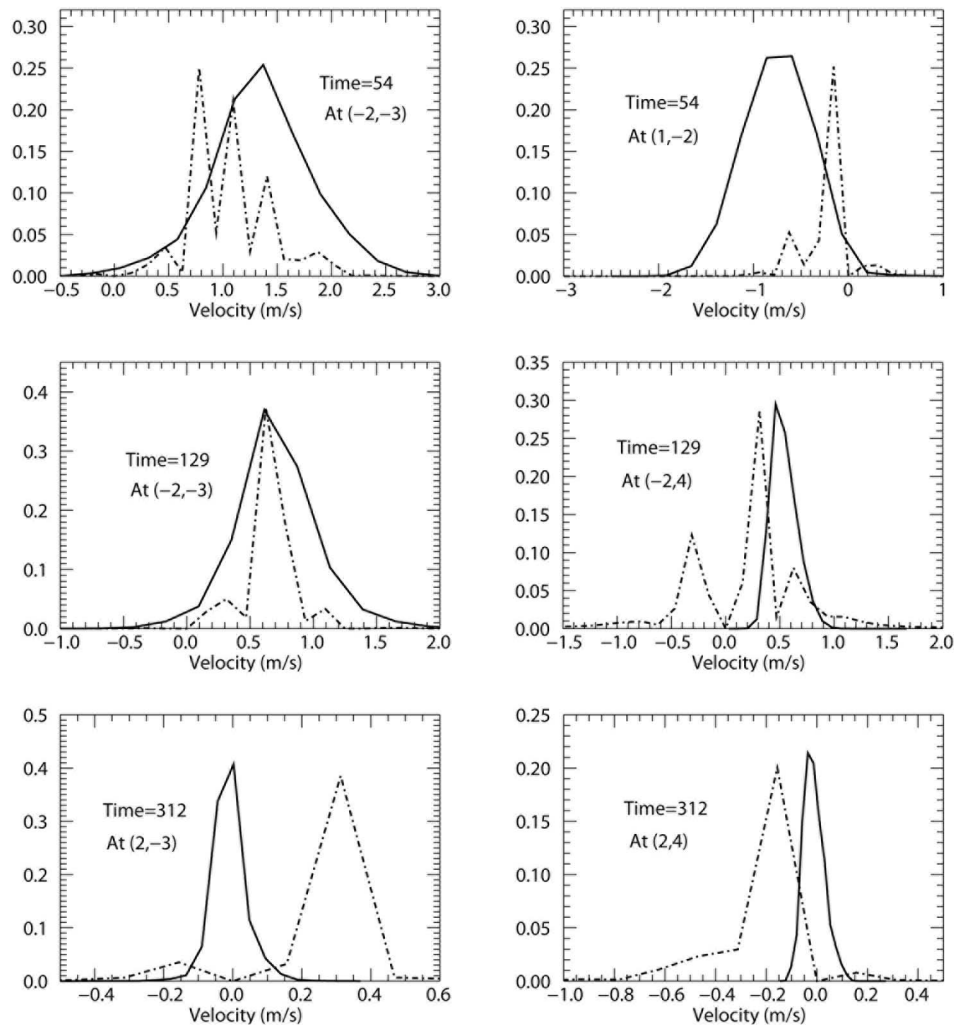


Figure 5. Same as Figure 3 but for the 10 MHz frequency and long pulse length of Case B.

distributions seen in Cases A and B at later times in several respects. First, peak power increases from comparable values at $t = 54$ to an ~ 2 times enhancement at $t = 129$ and 256 and an ~ 100 times enhancement at $t = 312$ and 364, Case C power also differs from Cases A and B in having power confined to the turbulence layer edge regions at $t = 256$ and beyond, where Case A had comparable power in the layer edge regions and center and Case B had peak power shifting from the edges to the center at later times. Elevated power levels at these times cause range cells both within and external to the turbulence layer to exhibit backscatter power below the 1% “measurement” threshold. Clearly, the 50 m Bragg scale in Case C is much better matched to the spatial scales of the refractive index variations than the 15 m Bragg scale in Cases A and B at these times.

[30] Vertical velocities for Case C, and their biases relative to the true velocities (see Figures 7c and 7d), are seen to be more similar to those discussed above for Case B than for Case A. Again, the longer radar pulse appears to enable somewhat better definition of the KH billow velocity structure at early and intermediate times. Doppler velocity errors are comparable in both magnitude and spatial distri-

bution to those seen in Case B out to $t = 129$. Thereafter, however, large biases in the turbulence layer edge regions, and outside it, yield velocity biases that become substantially larger than seen in either Case A or B (by factors of ~ 2 to 5). These biases are most pronounced, and of the same signs as seen in Cases A and B, in the turbulence layer edge regions. But their larger magnitudes imply a greater potential for misinterpretation of dynamics based on such measurements.

[31] As for Cases A and B, we display comparisons between radar Doppler spectra and the true velocity distributions within the same sampling volumes at early, intermediate, and later times ($t = 54, 129, \text{ and } 312$) in Figure 8. While the Doppler spectral resolution is ~ 3 times coarser in Case C (at 3 MHz) than in Cases A or B (at 10 MHz), similar common features and differences are observed. Spectral power is seen at Doppler velocities outside the range of true velocities at all times, biases in this case yield velocity estimates both larger and smaller than the corresponding true velocities (unlike the early and intermediate times for Cases A and B), and the extrema of the biases appear to increase with time (also noted in the discussion of

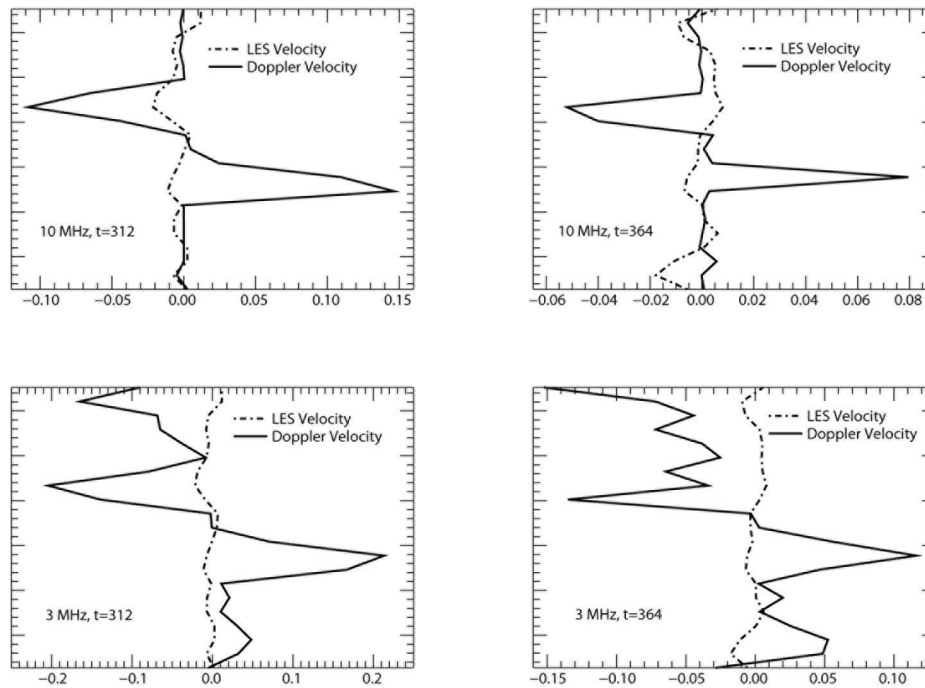


Figure 6. (top) Mean Doppler vertical velocities for the 10 MHz radar with 300 m pulse width (solid line) at (left) $t = 312$ and (right) $t = 364$ and the true LES velocities (dashed line) for the same sampling volumes and weighting (departures from zero reflect the nonuniform weighting of true velocities by the assumed radar beam pattern). (bottom) The same comparisons for the 3 MHz radar in Case C. Note that the mean biases are consistent with the individual Doppler spectra displayed in Figures 5 and 8.

Figure 7 above). The differences at later times are also apparent in the mean Doppler vertical velocity profiles displayed for Case C at $t = 312$ and 364 in Figure 6 (bottom). Comparing these profiles to the Figure 6 (top) panels for Case B, we see that the biases in Case C exhibit very similar structures in altitude, but are larger in magnitude and with peaks more extended in altitude (including outside the turbulence layer) than for the 10 MHz sampling frequency with the same pulse length and resolution.

[32] In most respects, the results obtained for Case C closely parallel those for the 10 MHz radar described in Cases A and B above. The velocity fields, spectra, and profiles arising in the three cases considered here indicate tendencies for both radar frequencies and pulse lengths (1) to capture the large-scale structure of the KH billow evolution up to the time of billow decay, (2) to underestimate the vertical velocities prior to billow decay, and (3) to experience biases in vertical velocity estimates following billow decay and accompanying restratification of the turbulence layer at late times. Despite capturing the large-scale flow structure, there are also clear systematic biases that arise and suggest that similar biases are likely present in real radar measurements of similar dynamics in the atmosphere.

5. Comparison With Previous Studies

[33] Our simulations of radar backscatter throughout the lifecycle of a KH instability exhibit many similarities to observed radar backscatter accompanying these dynamics throughout the atmosphere. The most obvious similarity is

between the simulated and observed power profiles, both of which exhibit the strongest responses surrounding active KH billows and at the edges of the turbulence layer following billow breakdown. Both observed and simulated backscatter power exhibit the Kelvin’s “cat’s eye” shape at early stages when the billows are clearly delineated [Browning, 1971; Gossard *et al.*, 1971; Fritts and Rastogi, 1985]. Well-resolved billow structures have also been observed from the boundary layer to the MLT [Eaton *et al.*, 1995; Woodman *et al.*, 2007; Lehmacher *et al.*, 2007; Luce *et al.*, 2008]. All suggest very little backscatter in the billow interiors, despite the clear evidence from our previous DNS studies and the current LES that the billow cores, and the interior of the turbulence layer, contain the most intense mechanical turbulence. Indeed, it is the mixing accompanying this turbulence that drives the maximum potential temperature gradients and wind shears to the edges of the billows and the subsequent turbulence layer. The stronger potential temperature gradients at the edge regions dominate the refractive index variations, and the radar backscatter power, extending to late times. Indeed, the negative correlation between backscatter power and turbulence intensity implied by these simulations also correspond closely to those observed or anticipated to lead to measurement biases in previous studies [see Hoppe *et al.*, 1990; Nastrom and VanZandt, 1994; Hoppe and Fritts, 1995a, 1995b; Tatarskii and Muschinski, 2001; Muschinski, 2004, and references therein]. The potential “bias” in the measurement of backscatter power is the suggestion that the billow cores and the subsequent turbulence layer may exhibit relatively smaller

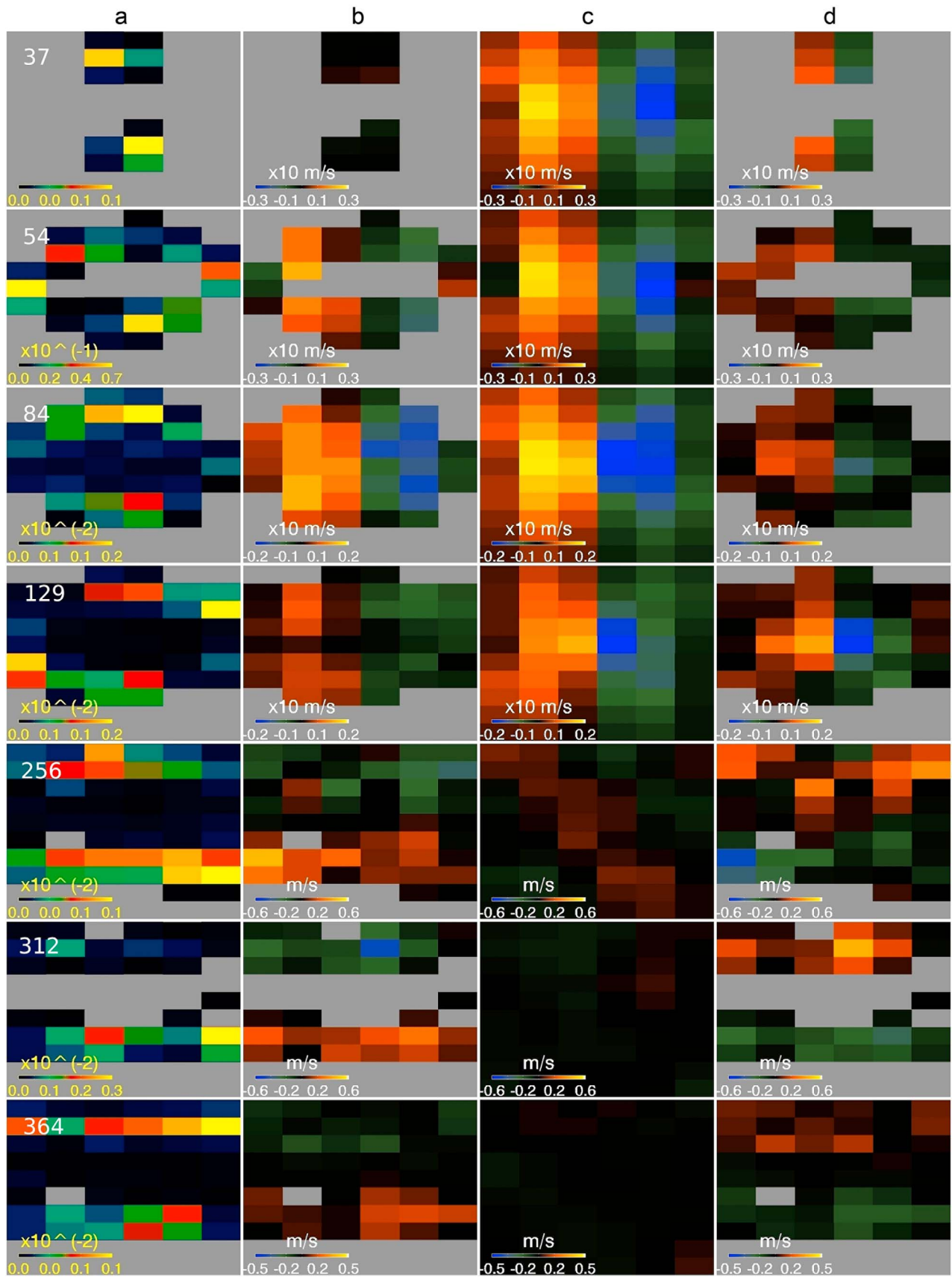


Figure 7. Same as Figure 2 but for a radar frequency of 3 MHz, a Bragg scale of $20 \Delta z$ (50 m), a pulse length of $120 \Delta z$ (vertical resolution of 150 m), and a beam width (FWHM) of 300 m.

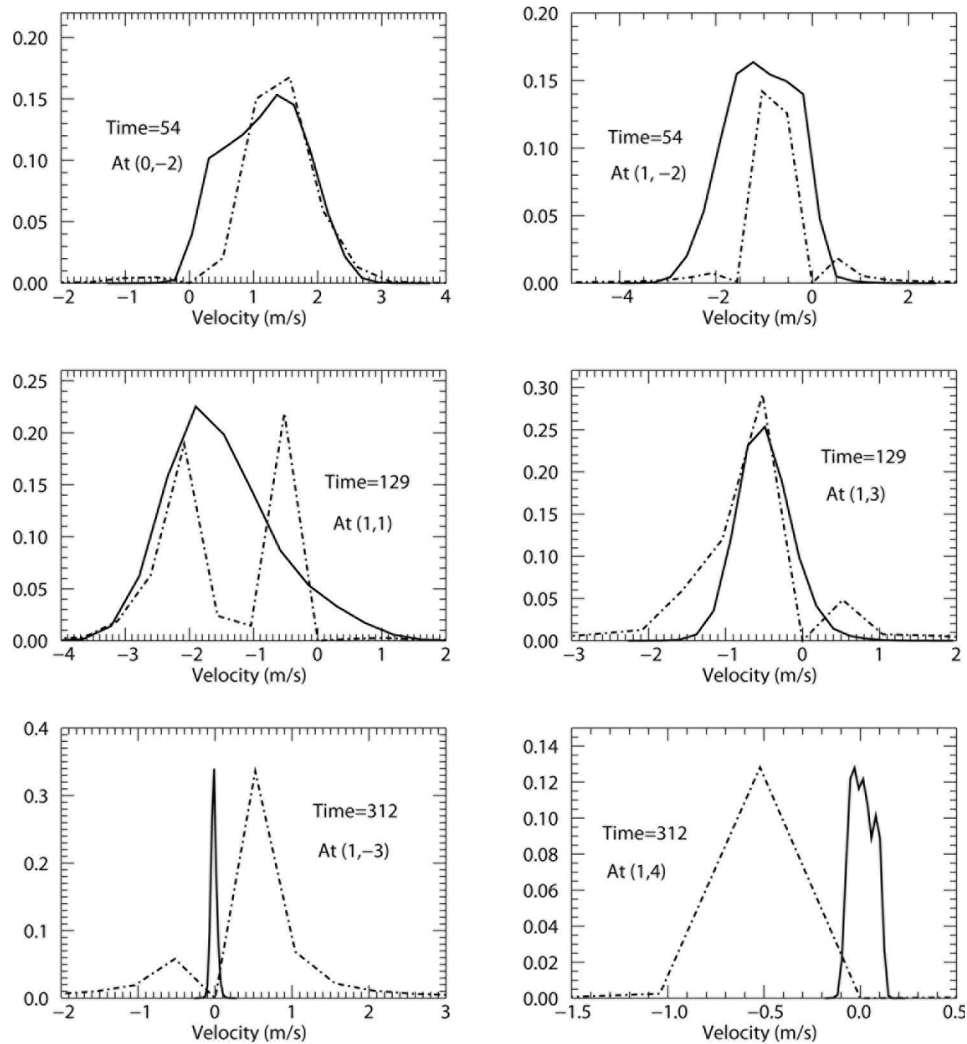


Figure 8. Same as Figure 5 but for the 3 MHz radar in Case C.

turbulence intensities and mixing than indicated by our previous DNS studies and the LES results shown in F11. This arises from the inability of most radars to measure turbulence spectral widths due to limited S/N within strong turbulence having very small refractive index gradients.

[34] Our radar backscatter simulations also demonstrate an expectation of radial velocity biases at various positions within KH billows and the subsequent turbulence layer throughout the KH lifecycle. These biases are difficult to compare with direct measurements of these dynamics, but our comparisons with the real radial velocities determined by our LES simulations reveal (1) insensitivity to velocities within the billow core, where strong mixing has largely eradicated the refractive index gradients, (2) a tendency to underestimate velocities where they are significant, especially within the billow cores, (3) potential biases in estimated velocities outside the billow and turbulence layer where refractive index variations are small, and (4) apparent vertical velocities at the edges of the turbulence layer at late times where persistent slanted structures having small slopes induce phase variations in radar backscatter due to hori-

zontal advection. Of the velocity measurement biases noted above, only the last was suggested by *Muschinski* [1996] prior to this study, and our results appear to confirm that suggestion. Specifically, persistent tilted structures accompanying large-scale shears appear likely to cause biased radial velocity estimates for both vertical and off-vertical beams for the reasons discussed above. The tendency for radial velocity estimates to be biased toward those portions of the billow having the largest refractive index fluctuations also suggests a potential for correlations of radial velocities and refractive index fluctuations that may bias mean velocity estimates in more general flows, as discussed by *Hoppe et al.* [1990], *Nastrom and VanZandt* [1994], *Hoppe and Fritts* [1995a, 1995b], *Tatarskii and Muschinski* [2001], and *Muschinski* [2004]. While we have not addressed Doppler spectral widths in this paper, we anticipate that, like the velocity estimates, such estimates may be biased toward those regions of the flow having the dominant refractive index fluctuations. For KH billows and the subsequent turbulence layers, this would likely yield a stronger weighting of the least turbulent and most stratified regions and overall

underestimates of spectral widths and turbulence intensities in cases with limited (finite) S/N.

6. Summary and Conclusions

[35] We have employed a high-resolution large-eddy simulation of the transition to, and evolution of, turbulence accompanying Kelvin-Helmholtz (KH) instability, and a general numerical description of radar backscatter from these turbulence fields, to assess the backscatter power and Doppler vertical velocities throughout the KH evolution. Our intentions were to provide descriptions of radar measurements of such dynamics to aid the interpretation of these dynamics seen by real radars and to note where radar measurements are likely to be absent, deficient, or biased because of either the radar method and/or assumptions, or the character of the scattering medium.

[36] For these purposes, we assumed a KH billow having a Richardson number $Ri = 0.05$, a Reynolds number $Re = 10,000$, a horizontal wavelength of ~ 1.8 km, and a depth of ~ 900 m, as these values are representative of KH parameters at MLT altitudes where our community expends considerable resources on such measurements. We computed 7 sequences of backscatter volumes spanning the KH instability evolution, each composed of 64 data sets spaced by 1.5 s and having a mesh of $720 \times 240 \times 1440$ spectral modes with a spatial resolution of 2.6 m, to allow Doppler spectra to be assembled for each sequence. These volumes extended from prior to and during the transition to turbulence, through the expansion of turbulence throughout the KH billow, and accompanying the billow and turbulence layer decay at late times. They thus allow radar Doppler spectra to be computed before turbulence arises, as well as at various stages of turbulence evolution, from transitional to fully developed to decaying and restratified. Three cases were examined, with the parameters for each given in Table 1.

[37] A summary of our results includes the following key findings.

[38] 1. The 10 MHz radar with a short pulse did a very good job of defining the KH billow morphology in the backscatter power profiles, where it was able to describe the characteristic cat's eye signature beginning before significant billow turbulence and extending to well after decay and restratification of the turbulence layer.

[39] 2. The 10 MHz radar with the short pulse provided only a qualitative description of the true vertical velocity field. Specifically, it failed to provide valid estimates within the billow core, the subsequent turbulence layer, or the external flow, and it exhibited significant biases at late times.

[40] 3. The 10 MHz radar with the medium pulse likewise described the KH billow morphology adequately in the power plots, but with less sensitivity to billow form and edges, much more variable backscatter power than obtained with the short pulse, and more returns in regions of the flow without high refractive index fluctuations.

[41] 4. The 10 MHz radar with the medium pulse was also able to provide somewhat better vertical velocity estimates than the same frequency with a shorter pulse at most locations across the KH billow and turbulence layer, beginning after turbulence formation and extending to late stages of restratification.

[42] 5. The 10 MHz radar, however, also tended to systematically underestimate the true vertical velocities at essentially all locations and to yield biased estimates at late times.

[43] 6. The 3 MHz radar performed much more like the 10 MHz radar having the same (medium) pulse length. It was able to describe the large-scale KH dynamics fairly realistically, it captured the KH cat's eye signature morphology, but it underestimated true vertical velocities following turbulence formation; it also exhibited biases at late times consistent with those seen at 10 MHz, but led to larger maximum velocity errors than seen at 10 MHz with either pulse length.

[44] 7. Backscatter power for both radar frequencies and pulse lengths was seen to be maximum in regions of the flow having large thermal and refractive index gradients and relatively small turbulence intensities, suggesting (1) a strong anticorrelation between backscatter power and turbulence spectral widths and intensities and (2) systematic underestimates of turbulence energy dissipation based on measured spectral widths.

[45] 8. Biased vertical velocities obtained with the 3 and 10 MHz radars at late times arose due to specular backscatter due to tilted surfaces in the restratifying turbulence flow that were significant when true vertical velocities were very small.

[46] The bottom line is that our virtual radars performed sufficiently well to identify the KH instability dynamics underlying radar backscatter from early in the turbulence transition through billow collapse, formation of a quasi-homogeneous turbulence layer, and its subsequent restratification. There were, nevertheless, clear biases in assessments of backscatter power and Doppler vertical velocities due to the character and distribution of the associated thermal and refractive index gradients at various stages of the KH evolution. Systematic underestimates of true vertical velocities within the KH billows suggest less than full quantification of such events by real radars. Biases in vertical velocity estimates as large as ~ 0.1 to 0.2 m s^{-1} due to specular reflections from slanted structures at late stages suggest a potential for systematic biases in estimates of mean vertical motions, and likely in the vertical profiles of horizontal winds with off-zenith beams. Such biases would be proportionately larger for larger-scale KH billows than assumed in our discussion here. Though these results were obtained for sampling frequencies lower than employed for typical radars making such measurements, we anticipate these results to be indicative of what is seen at higher frequencies because of the character at the various stages of the KH instability and turbulence evolution. Additional aspects of radar backscatter from realistic turbulence data to be addressed in future papers will include aspect sensitivity, turbulence due to breaking gravity waves, and biases accompanying correlations of turbulence character with the larger-scale motion field.

[47] **Acknowledgments.** This research was supported under NASA contracts NAS5-02069 and NAG5-02036 and NSF grants ATM-0138982, ATM-0240829, ATM-0314060, ATM-0435789, and ATM-0750929.

References

- Balsley, B. B., and K. S. Gage (1980), The MST radar technique: Potential for middle atmospheric studies, *Pure Appl. Geophys.*, *118*(1), 452–493, doi:10.1007/BF01586464.
- Balsley, B. B., and A. C. Riddle (1984), Monthly mean values of the mesospheric wind field over Poker Flat, Alaska, *J. Atmos. Sci.*, *41*, 2368–2380, doi:10.1175/1520-0469(1984)041<2368:MMVOTM>2.0.CO;2.
- Blumen, W., R. Banta, S. P. Burns, D. C. Fritts, R. Newsom, G. S. Poulos, and J. Sun (2001), Turbulence statistics of a Kelvin-Helmholtz billow event observed in the nighttime boundary layer during the CASES-99 field program, *Dyn. Atmos. Oceans*, *34*, 189–204, doi:10.1016/S0377-0265(01)00067-7.
- Bolgiano, R., Jr. (1959), Turbulent spectra in a stably stratified atmosphere, *J. Geophys. Res.*, *64*, 2226–2229, doi:10.1029/JZ064i012p02226.
- Bolgiano, R., Jr. (1962), Structure of turbulence in stratified media, *J. Geophys. Res.*, *67*, 3015–3023, doi:10.1029/JZ067i008p03015.
- Browne, L. W. B., A. A. Antonia, and D. A. Shaw (1987), Turbulent energy dissipation in a wake, *J. Fluid Mech.*, *179*, 307–326, doi:10.1017/S002211208700154X.
- Browning, K. A. (1971), Structure of the atmosphere in the vicinity of large-amplitude Kelvin-Helmholtz billows, *Q. J. R. Meteorol. Soc.*, *97*, 283–299, doi:10.1002/qj.49709741304.
- Champagne, F. H. (1978), The fine-scale structure of the turbulent velocity field, *J. Fluid Mech.*, *86*, 67–108, doi:10.1017/S0022112078001019.
- Chilson, P. B., A. Muschinski, and G. Schmidt (1997), First observations of Kelvin-Helmholtz billows in an upper-level jet stream using VHF frequency domain interferometry, *Radio Sci.*, *32*, 1149–1160, doi:10.1029/97RS00088.
- Cho, J. Y. N., and J. Röttger (1997), An updated review of polar mesosphere summer echoes: Observation, theory, and their relationship to noctilucent clouds and subvisible aerosols, *J. Geophys. Res.*, *102*, 2001–2020, doi:10.1029/96JD02030.
- Doviak, R. J., and D. S. Zmick (1984), Reflection and scatter formula for anisotropically turbulent air, *Radio Sci.*, *19*, 325–336, doi:10.1029/RS019i001p00325.
- Durbin, P. A., and C. G. Speziale (1991), Local anisotropy in strained turbulence at high Reynolds numbers, *ASME J. Fluids Eng.*, *113*, 707–709, doi:10.1115/1.2926540.
- Eaton, F. D., S. A. McLaughlin, and J. R. Hines (1995), A new frequency-modulated continuous wave radar for studying planetary boundary layer morphology, *Radio Sci.*, *30*, 75–88, doi:10.1029/94RS01937.
- Franke, P. M., S. Mahmoud, K. Wan, D. C. Fritts, T. Lund, and J. Werne (2011), Computation of clear-air radar backscatter from numerical simulations of turbulence: 1. Numerical methods and evaluation of biases, *J. Geophys. Res.*, doi:10.1029/2010JD015895, in press.
- Fritts, D. C., and M. J. Alexander (2003), Gravity dynamics and effects in the middle atmosphere, *Rev. Geophys.*, *41*(1), 1003, doi:10.1029/2001RG000106.
- Fritts, D. C., and P. K. Rastogi (1985), Convective and dynamical instabilities due to gravity wave motions in the lower and middle atmosphere: Theory and observations, *Radio Sci.*, *20*, 1247–1277, doi:10.1029/RS020i006p01247.
- Fritts, D. C., and L. Yuan (1989), Measurement of momentum fluxes near the summer mesopause at Poker Flat, Alaska, *J. Atmos. Sci.*, *46*, 2569–2579, doi:10.1175/1520-0469(1989)046<2569:MOMFNT>2.0.CO;2.
- Fritts, D. C., U.-P. Hoppe, and B. Inhester (1990), A study of the vertical motion field near the high-latitude summer mesopause during MAC/SINE, *J. Atmos. Terr. Phys.*, *52*, 927–938, doi:10.1016/0021-9169(90)90025-1.
- Fritts, D. C., T. L. Palmer, Ø. Andreassen, and I. Lie (1996), Evolution and breakdown of Kelvin-Helmholtz billows in stratified compressible flows: I. Comparison of two- and three-dimensional flows, *J. Atmos. Sci.*, *53*, 3173–3191, doi:10.1175/1520-0469(1996)053<3173:EABOKB>2.0.CO;2.
- Fritts, D. C., C. Bizon, J. A. Werne, and C. K. Meyer (2003), Layering accompanying turbulence generation due to shear instability and gravity wave breaking, *J. Geophys. Res.*, *108*(D8), 8452, doi:10.1029/2002JD002406.
- Fritts, D. C., L. Wang, J. Werne, T. Lund, and K. Wan (2009a), Gravity wave instability dynamics at high Reynolds numbers, 1: Wave field evolution at large amplitudes and high frequencies, *J. Atmos. Sci.*, *66*, 1126–1148, doi:10.1175/2008JAS2726.1.
- Fritts, D. C., L. Wang, J. Werne, T. Lund, and K. Wan (2009b), Gravity wave instability dynamics at high Reynolds numbers: 2. Turbulence evolution, structure, and anisotropy, *J. Atmos. Sci.*, *66*, 1149–1171, doi:10.1175/2008JAS2727.1.
- Fukao, S., M. F. Larsen, M. D. Yamanaka, H. Furukawa, T. Tsuda, and S. Kato (1991), Observations of a reversal in long-term average vertical velocities near the jet-stream wind maximum, *Mon. Weather Rev.*, *119*, 1479–1489, doi:10.1175/1520-0493(1991)119<1479:OOARIL>2.0.CO;2.
- Gibson-Wilde, D. E., J. A. Werne, D. C. Fritts, and R. J. Hill (2000), Direct numerical simulation of VHF radar measurements of turbulence in the mesosphere, *Radio Sci.*, *35*, 783–798, doi:10.1029/1999RS002269.
- Gossard, E. E., D. R. Jensen, and J. H. Richter (1971), An analytical study of tropospheric structure as seen by high-resolution radar, *J. Atmos. Sci.*, *28*, 794–807, doi:10.1175/1520-0469(1971)028<0794:AASOTS>2.0.CO;2.
- Hecht, J. H. (2004), Instability layers and airglow imaging, *Rev. Geophys.*, *42*, RG1001, doi:10.1029/2003RG000131.
- Hecht, J. H., A. Z. Liu, R. L. Walterscheid, and R. J. Rudy (2005), Maui Mesosphere and Lower Thermosphere (Maui MALT) observations of the evolution of Kelvin-Helmholtz billows formed near 86 km altitude, *J. Geophys. Res.*, *110*, D09S10, doi:10.1029/2003JD003908.
- Hill, R. J., and K. A. Mitton (1998), Turbulence-induced ionization fluctuations in the lower ionosphere, *NOAA Tech. Rep. ERL 454-ETL 68*, 112 pp., Natl. Tech. Inf. Serv., Springfield, Va.
- Hill, R. J., D. E. Gibson-Wilde, J. A. Werne, and D. C. Fritts (1999), Turbulence-induced fluctuations in ionization and application to PMSE, *Earth Planets Space*, *51*, 499–513.
- Hoppe, U.-P., and D. C. Fritts (1995a), On the downward bias in vertical velocity measurements by VHF radars, *Geophys. Res. Lett.*, *22*, 619–622, doi:10.1029/95GL00165.
- Hoppe, U.-P., and D. C. Fritts (1995b), High-resolution measurements of vertical velocity with the EISCAT VHF radar: 1. Motion field characteristics and measurement biases, *J. Geophys. Res.*, *100*, 16,813–16,825, doi:10.1029/95JD01466.
- Hoppe, U.-P., D. C. Fritts, I. M. Reid, P. Czechowsky, C. M. Hall, and T. L. Hansen (1990), Multiple-frequency studies of the high-latitude summer mesosphere: Implications for scattering processes, *J. Atmos. Terr. Phys.*, *52*, 907–926, doi:10.1016/0021-9169(90)90024-H.
- Hunt, J. C. R., O. M. Phillips, and D. Williams (1991), Turbulence and stochastic processes: Kolmogorov's ideas 50 years on, *Proc. R. Soc. A*, *434*, 240 pp.
- Kelley, M. C., C. Y. Chen, R. R. Beland, R. Woodman, J. L. Chau, and J. Werne (2005), Persistence of a Kelvin-Helmholtz instability complex in the upper troposphere, *J. Geophys. Res.*, *110*, D14106, doi:10.1029/2004JD005345.
- Klaassen, G. P., and W. R. Peltier (1985), The onset of turbulence in finite-amplitude Kelvin-Helmholtz billows, *J. Fluid Mech.*, *155*, 1–35, doi:10.1017/S0022112085001690.
- Klaassen, G. P., and W. R. Peltier (1991), The influence of stratification on secondary instabilities in free shear layers, in finite-amplitude Kelvin-Helmholtz billows, *J. Fluid Mech.*, *227*, 71–106, doi:10.1017/S0022112091000046.
- Kudeki, E., P. K. Rastogi, and F. Surucu (1993), Systematic errors in radar wind estimation: Implications for comparative measurements, *Radio Sci.*, *28*, 169–179, doi:10.1029/92RS01931.
- Lehmacher, G. A., L. Guo, E. Kudeki, P. M. Reyes, A. Akgiray, and J. Chou (2007), High-resolution observations of mesospheric layers with the Jicamarca VHF radar, *Adv. Space Res.*, *40*(6), 734–743, doi:10.1016/j.asr.2007.05.059.
- Lübken, F.-J., M. Rapp, T. Blix, and E. Thrane (1998), Microphysical and turbulent measurements of the Schmidt number in the vicinity of polar mesosphere summer echoes, *Geophys. Res. Lett.*, *25*, 893–896, doi:10.1029/98GL50479.
- Luce, H., G. Hassenpflug, M. Yamamoto, M. Crochet, and S. Fukao (2007), Range-imaging observations of cumulus convection and Kelvin-Helmholtz instabilities with the MU radar, *Radio Sci.*, *42*, RS1005, doi:10.1029/2005RS003439.
- Luce, H., G. Hassenpflug, M. Yamamoto, S. Fukao, and K. Sato (2008), High-resolution observations with MU radar of a KH instability triggered by an inertia-gravity wave in the upper part of a jet stream, *J. Atmos. Sci.*, *65*, 1711–1718, doi:10.1175/2007JAS2346.1.
- Lumley, J. L. (1964), The spectrum of nearly inertial turbulence in a stably stratified fluid, *J. Atmos. Sci.*, *21*, 99–102, doi:10.1175/1520-0469(1964)021<0099:TSONIT>2.0.CO;2.
- Meek, C. E., and A. H. Manson (1989), Vertical motions in the upper middle atmosphere from the Saskatoon (52°N, 107°W) M. F. radar, *J. Atmos. Sci.*, *46*, 849–858, doi:10.1175/1520-0469(1989)046<0849:VMITUM>2.0.CO;2.
- Mestayer, P. (1982), Local isotropy and anisotropy in a high Reynolds turbulent boundary layer, *J. Fluid Mech.*, *125*, 475–503, doi:10.1017/S0022112082003450.
- Muschinski, A. (1996), Possible effect of Kelvin-Helmholtz instability on VHF radar observations of the mean vertical wind, *J. Appl. Meteorol.*, *35*, 2210–2217, doi:10.1175/1520-0450(1996)035<2210:PEOKHI>2.0.CO;2.

- Muschinski, A. (2004), Local and global statistics of clear-air Doppler radar signals, *Radio Sci.*, *39*, RS1008, doi:10.1029/2003RS002908.
- Muschinski, A., P. P. Sullivan, D. B. Wuerz, R. J. Hill, S. A. Cohn, D. H. Lenschow, and R. J. Doviak (1999), First synthesis of wind-profiler signals on the basis of large-eddy simulation data, *Radio Sci.*, *34*, 1437–1460, doi:10.1029/1999RS000090.
- Nastrom, G. D., and T. E. VanZandt (1994), Mean vertical motions seen by radar wind profilers, *J. Appl. Meteorol.*, *33*, 984–995, doi:10.1175/1520-0450(1994)033<0984:MVMSBR>2.0.CO;2.
- Nastrom, G. D., W. L. Ecklund, and K. S. Gage (1985), Direct measurement of large-scale vertical velocities using clear-air Doppler radars, *Mon. Weather Rev.*, *113*, 708–718, doi:10.1175/1520-0493(1985)113<0708:DMOLVV>2.0.CO;2.
- Peltier, W. R., and C. P. Caulfield (2003), Mixing efficiency in stratified shear flows, *Annu. Rev. Fluid Mech.*, *35*, 135–167, doi:10.1146/annurev.fluid.35.101101.161144.
- Petersson-Reif, B. A., and Ø. Andreassen (2003), On local isotropy in stratified homogeneous turbulence, *SIAM J. Appl. Math.*, *64*(1), 309–321, doi:10.1137/S0036139903421559.
- Petersson-Reif, B. A., J. Werne, Ø. Andreassen, C. Meyer, and M. Davis-Mansour (2002), Entrainment-zone restratification and flow structures in stratified shear turbulence, in *Studying Turbulence Using Numerical Simulation Databases - IX, Proceedings of the 2002 CTR Summer Program*, edited by P. Bradshaw, pp. 245–256, Cent. for Turbulence Res., Stanford Univ., Stanford, Calif.
- Röttger, J. (1994), Polar mesosphere summer echoes: Dynamics and aeronomy of the mesosphere, *Adv. Space Res.*, *14*, 123–137.
- Røyrvik, Ø. (1983), VHF radar signals scattered from the equatorial mesosphere, *Radio Sci.*, *18*, 1325–1335, doi:10.1029/RS018i006p01325.
- Ruggiero, F. H., J. Werne, T. S. Lund, D. C. Fritts, K. Wan, L. Wang, A. Mahalov, and B. Nichols (2005), Characterization of high altitude turbulence for Air Force platforms, paper presented at 15th DoD HPC User Group Conference, Dep. of Defense, Nashville, Tenn.
- Rüster, R., and I. M. Reid (1990), VHF radar observations of the dynamics of the summer polar mesopause region, *J. Geophys. Res.*, *95*, 10,005–10,016, doi:10.1029/JD095iD07p10005.
- Smyth, W. D. (1999), Dissipation-range geometry and scalar spectra in sheared stratified turbulence, *J. Fluid Mech.*, *401*, 209–242, doi:10.1017/S0022112099006734.
- Smyth, W. D., and J. N. Moum (2000), Anisotropy of turbulence in stably stratified mixing layers, *Phys. Fluids*, *12*, 1343–1362, doi:10.1063/1.870386.
- Sreenivasan, K. R. (1991), On local isotropy of passive scalars in turbulent shear flows, *Proc. R. Soc. A*, *434*, 165–182, doi:10.1098/rspa.1991.0087.
- Tatarskii, V. I. (1961), *Wave Propagation in a Turbulent Medium*, McGraw-Hill, New York.
- Tatarskii, V. I. (1971), The effect of the turbulent atmosphere wave propagation, translated from Russian, 472 pp., Isr. Program for Sci. Transl., Jerusalem.
- Tatarskii, V. I., and A. Muschinski (2001), The difference between Doppler velocity and real wind velocity in single scattering from refractive index fluctuations, *Radio Sci.*, *36*, 1405–1423, doi:10.1029/2000RS002376.
- Thorpe, S. A. (1973a), Experiments on instability and turbulence in a stratified shear flow, *Boundary Layer Meteorol.*, *5*, 95–119, doi:10.1007/BF02188314.
- Thorpe, S. A. (1973b), Turbulence in stably stratified fluids: A review of laboratory experiments, *J. Fluid Mech.*, *61*, 731–751, doi:10.1017/S0022112073000911.
- Thorpe, S. A. (1987), Transitional phenomena and the development of turbulence in stratified fluids: A review, *J. Geophys. Res.*, *92*, 5231–5248, doi:10.1029/JC092iC05p05231.
- Townsend, A. A. (1959), The uniform distortion of homogeneous turbulence, *Q. J. Mech. Appl. Math.*, *28*, 104–127.
- Uberoi, M. S. (1957), Equipartitioning of energy and local isotropy in turbulent flows, *J. Appl. Phys.*, *28*, 1165–1170, doi:10.1063/1.1722600.
- Van Atta, C. (1991), Local isotropy of the smallest scales of turbulent scalar and velocity fields, *Proc. R. Soc. A*, *434*, 139–147, doi:10.1098/rspa.1991.0085.
- Wang, D.-Y., and D. C. Fritts (1990), Mesospheric momentum fluxes observed by the MST radar at Poker Flat, Alaska, *J. Atmos. Sci.*, *47*, 1512–1521, doi:10.1175/1520-0469(1990)047<1512:MMFOBT>2.0.CO;2.
- Weinstock, J. (1981), Energy dissipation rates of turbulence in the stable free atmosphere, *J. Atmos. Sci.*, *38*, 880–883, doi:10.1175/1520-0469(1981)038<0880:EDROTT>2.0.CO;2.
- Werne, J. A., and D. C. Fritts (1999a), Stratified shear turbulence: Evolution and statistics, *Geophys. Res. Lett.*, *26*, 439–442, doi:10.1029/1999GL900022.
- Werne, J. A., and D. C. Fritts (1999b), Anisotropy in stratified shear turbulence, paper presented at 9th DoD HPC User Group Symposium, Dep. of Defense, Monterey, Calif.
- Werne, J. A., and D. C. Fritts (2000), Structure functions in stratified shear turbulence, paper presented at 10th DoD HPC User Group Symposium, Dep. of Defense, Albuquerque, N. M.
- Werne, J. A., and D. C. Fritts (2001), Anisotropy in a stratified shear layer, *Phys. Chem. Earth*, *26*, 263–268.
- Werne, J., T. Lund, B. A. Petersson-Reif, P. Sullivan, and D. C. Fritts (2005), CAP Phase II simulations for the Air Force HEL-JTO project, paper presented at 15th DoD HPCMP Users Group Conference, Dep. of Defense, Nashville, Tenn.
- Witt, G. (1962), Height, structure, and displacements of noctilucent clouds, *Tellus*, *14*, 1–18, doi:10.1111/j.2153-3490.1962.tb00115.x.
- Woodman, R. F., G. Michhue, J. Roettger, and O. Castillo (2007), The SOUSY radar at Jicamarca: High altitude-resolution capabilities, paper presented at MST-11 Workshop, Natl. Atmos. Res. Lab., Gadanki, India.
- Woods, J. D., and R. L. Wiley (1972), Billow turbulence and ocean microstructure, *Deep Sea Res.*, *19*, 87–121.
- Worthington, R. M., A. Muschinski, and B. B. Balsley (2001), Bias in mean vertical wind measured by VHF radars: Significance of radar location relative to mountains, *J. Atmos. Sci.*, *58*, 707–723, doi:10.1175/1520-0469(2001)058<0707:BIMVWM>2.0.CO;2.
- Wroblewski, D., O. Cote, J. Hacker, T. L. Crawford, and R. J. Dobosy (2003), Refractive turbulence in the upper troposphere and lower stratosphere: Analysis of aircraft measurements using structure functions, paper presented at 12th Symposium on Meteorological Observations and Instrumentation, Am. Meteorol. Soc., Long Beach, Calif.

P. M. Franke, Department of Electrical and Computer Engineering, University of Illinois at Urbana-Champaign, Urbana, IL 61801, USA.

D. C. Fritts, T. Lund, K. Wan, and J. Werne, Colorado Research Associates Division, NorthWest Research Associates, 3380 Mitchell Ln., Boulder, CO 80301, USA. (dave@cora.nwra.com)